Supplementary Information:

Width-Dependent Band Gap in Armchair Graphene Nanoribbons Reveals Fermi Level Pinning on Au(111).

Néstor Merino-Díez,[‡,†] *Aran Garcia-Lekue,*[‡,§], *Eduard Carbonell-Sanromà,*[†] *Jincheng Li,*[⊥,†] *Martina Corso,*[†,§,⊥] *Luciano Colazzo,*[▽] *Francesco Sedona,*[▽] *Daniel Sánchez-Portal,*[‡,⊥] *Jose I. Pascual,*[†,§] *and Dimas G. de Oteyza*[‡,§,⊥].

[‡]Donostia International Physics Center (DIPC), 20018 Donostia – San Sebastián, Spain

[†]CIC nanoGUNE, Nanoscience Cooperative Research Center, 20018 Donostia – San Sebastián, Spain

[§] Ikerbasque, Basque Foundation for Science, 48013 Bilbao, Spain

[⊥] Centro de Física de Materiales (CSIC/UPV-EHU) - Materials Physics Center, 20018 Donostia – San Sebastián, Spain

[▽] Dipartimento di Scienze Chimiche, Università di Padova, 35131 Padova, Italy

Author(s) address: d_g_oteyza@ehu.es

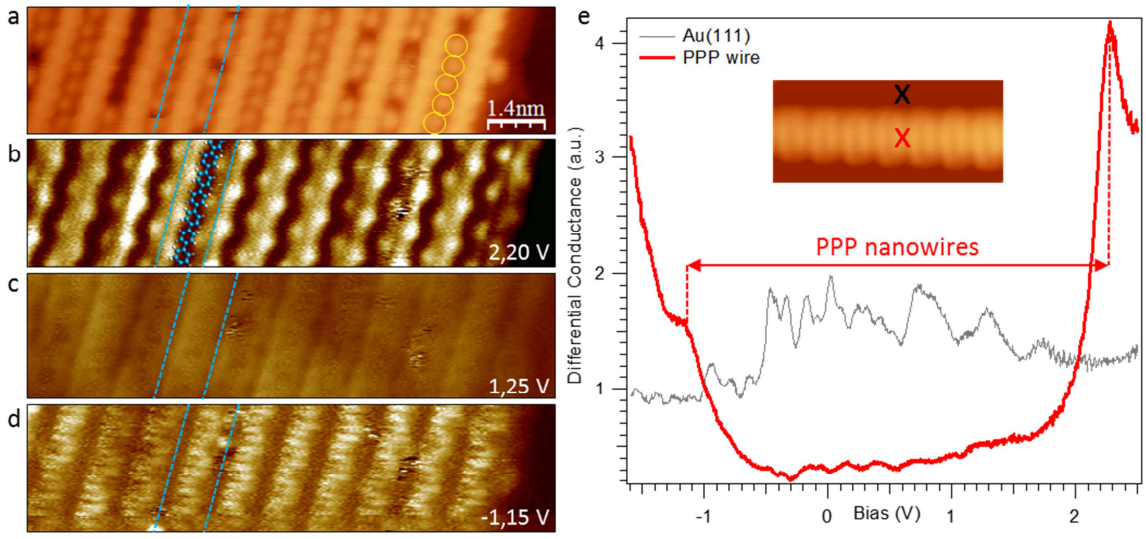

Figure S1. (a) STM topography image (12.3 nm x 2.9nm; V_s = -1.1 V; I_t = 0.60 nA). Conductance maps (12.3 nm x 2.9nm; I_t = 0.60 nA) on PPP wires at **(b)** valence band edge (V_s = 2.20 V), where simulated representation of PPP wire is included as visual guide; **(c)** within the band gap (V_s = 1.25 V), and **(d)** at conduction band edge (V_s = -1.15 V). Blue lines superimposed to the adsorbated Br atoms (yellow circles) to the substrate are included for an easier appreciation of single nanowire features. **(e)** Spectra taken on PPP nanowires (in red) where Au(111) signal (in black) is added to every spectrum as background reference (open-feed-back parameters: V_s = -1.60 V; I_t = 0.54 nA; modulation voltage V_{rms} = 18 V). Crosses in inset topographic image indicate the positions where spectra were recorded.

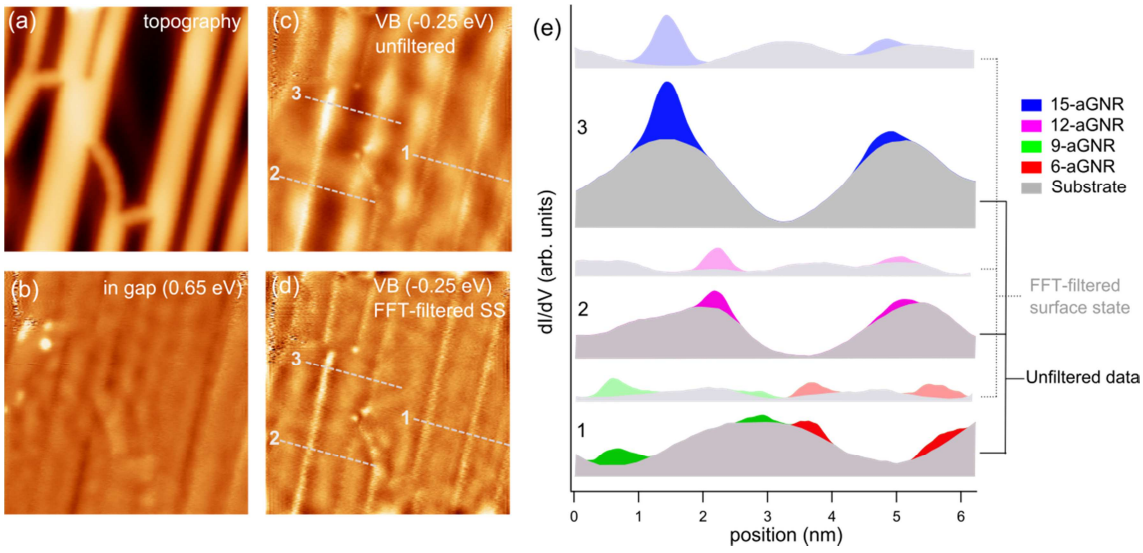

Figure S2. (a) STM topography image (12,4 nm x 12.4 nm; V_s = -1.1 V; I_t = 0.61 nA) displaying GNRs of varying width. **(b)** Conductance map at an energy within the band gap (V_s = 0.65 V), revealing the absence of GNR-related signal and only the oscillations from the scattered Au surface state. **(c)** Conductance map near the valence band onset (V_s = -0.25 V). The three numbered lines mark the position of profiles taken so as to cross GNRs of the different studied widths. **(d)** Same conductance map as in (c) but after filtering the main surface state signal. To do so, an FFT image of (c) is calculated, the k corresponding to the surface state is cut and then the image is transformed back. Without most of the substrate-related signal,the overall corrugation is lowered, making it easier to distinguish the GNR-related signal **(e)** Profiles across the conductance maps in (c) and (d), highlighting the contribution from the VB of differently wide GNRs on top of the underlying substate contribution. Comparing the profiles on filtered and unfiltered conductance images one can clearly distinguish how by applying the filter the GNR signal remains unaltered on top of a substantially less corrugated substrate signal, overall making its distinction easier.

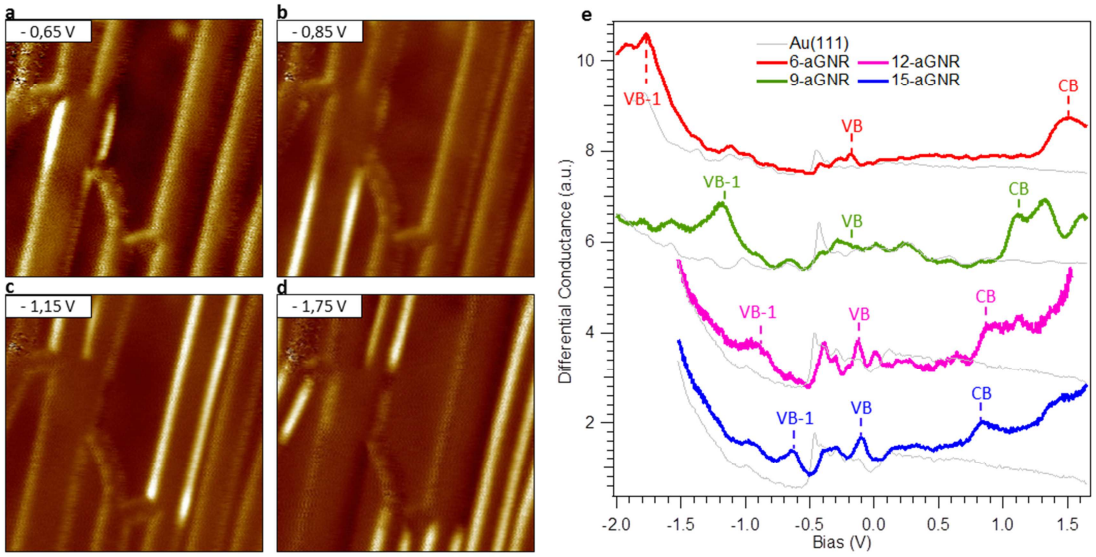

Figure S3. (a-d) Conductance maps (12.4 nm x 12.4 nm; I_t = 0.60 nA) at the onsets of the second valence bands (VB-1) on **(a)** 15-aGNR (V_s = -0.65 V), **(b)** 12-aGNR (V_s = -0.85 V), **(c)** 9-aGNR (V_s = -1.15 V) and **(d)** 6-aGNR (V_s = -1.75 V). **(e)** Spectra taken on 6-aGNR (in red), 9-aGNR (in green), 12-aGNR (in pink) and 15-aGNR (in blue) where Au(111) signal (in black) is added to every spectrum as background reference (open-feed-back parameters: V_s= -1.0 V; I_t = 0.5–10 nA; modulation voltage V_{rms} = 10-12 mV).

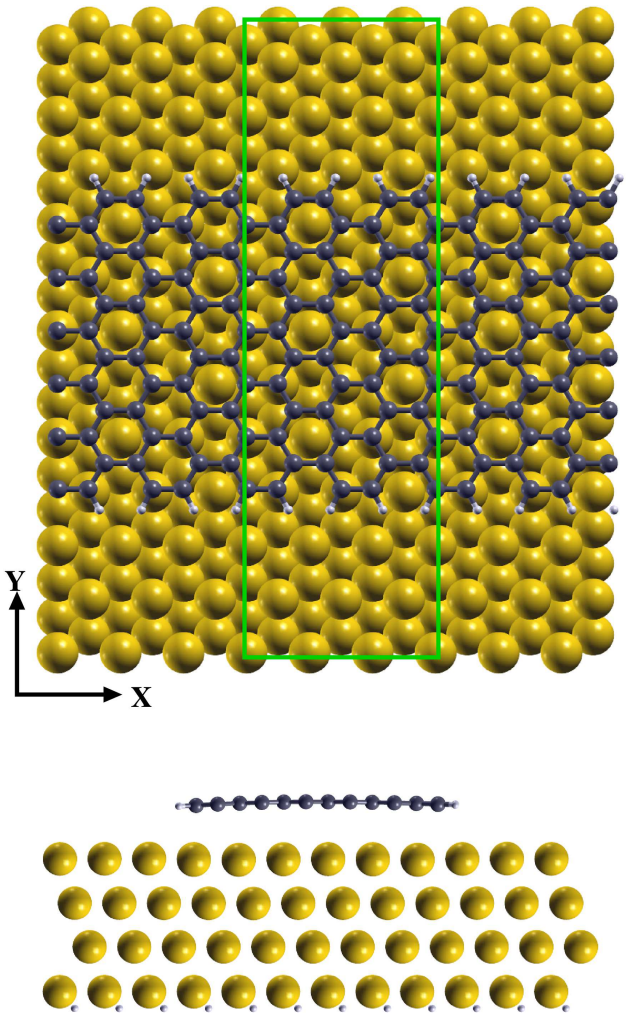

Figure S4. Example of one of the setups used for the calculations: graphene nanoribbon of 12 dimer lines on a Au(111) slab with a lateral unit cell as indicated by the green rectangle. The ribbon is periodic along the X direction.

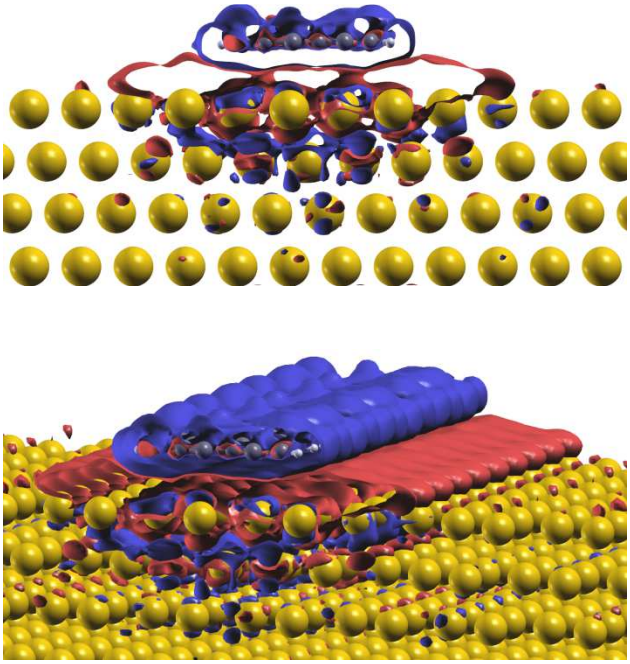

Figure S5. Iso-surface (5×10^{-4} electrons/bohr^3) of the computed induced charge upon adsorption of a 6-aGNR on Au(111). **Top:** front view. **Bottom:** side view. Red surfaces correspond to electron accumulation, while blue surfaces correspond to electron depletion. Pauli repulsion by the ribbon electrons pushes the electrons of gold towards the surface, giving rise to a modification of the surface dipole. As clearly shown in the image, the electron accumulation spills out from the region covered by the ribbon, modifying the surface dipole with respect to that of extended graphene. The modification will be larger the narrower the ribbon.

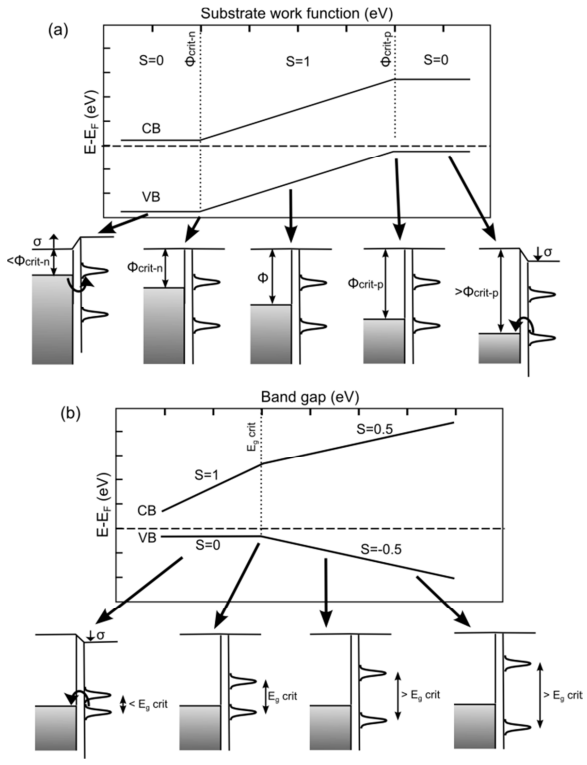

Figure S6. **(a)** Schematic model of the changing energy level alignment of weakly interacting adsorbate´s valence and conduction bands with varying work function of the substrate. The alignment changes from vacuum level pinning to Fermi level pinning of valence and conduction bands at critically high and low work functions, respectively. Analyzing the slope S of the energy level alignment changes vs. the work function, this translates in changes from S=1 for vacuum level pinning to S=0 for Fermi level pinning. **(b)** Schematic model of the changing energy level alignment of weakly interacting adsorbate´s valence and conduction bands with varying band gap. As the band gap is reduced, the valence and conduction band onsets move symmetrically towards the mid-gap value with a slope S=0.5. As one of the bands gets sufficiently close to Fermi, Fermi level pinning of that band sets in (valence band in the picture, S=0) and only the non-pinned band supports the full band gap change henceforth, shifting accordingly with a slope of S=1.

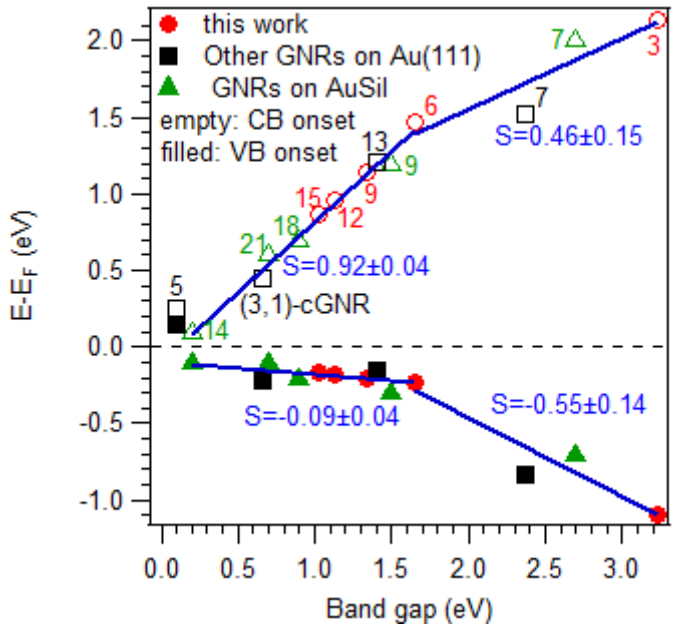

Figure S7. Valence and conduction band onsets of GNRs studied in this work and in other reports of Au(111)-supported ribbons vs. their respective band gap (width given by the numbers next to CB symbols). Data of GNRs on an even less interactive substrate as is a Si intercalated layer on Au(111) are also added for comparison. Linear fits in selected regions display the changes in slope, evidencing remarkable similarity with the model scenario of Fig. S6b. The data not corresponding to this work have been taken from references [1] (7-aGNR/Au(111)), [2] (9-aGNR/Au(111)), [3] ((3,1)-cGNR/Au(111)), [4] (5-aGNR/Au(111)) and [5] (aGNRs/AuSil).

References

(1) Söde, H.; Talirz, L.; Gröning, O.; Pignedoli, C. A.; Berger, R.; Feng, X.; Müllen, K.; Fasel, R.; Ruffieux, P. Electronic Band Dispersion of Graphene Nanoribbons via Fourier-Transformed Scanning Tunneling Spectroscopy. *Physical Review B* **2015**, *91*, 045429.

(2) Talirz, L.; Söde, H.; Dumslaff, T.; Wang, S.; Sanchez-Valencia, J. R.; Liu, J.; Shinde, P.; Pignedoli, C. A.; Liang, L.; Meunier, V.; *et al.* On-Surface Synthesis and Characterization of 9-Atom Wide Armchair Graphene Nanoribbons. *ACSnano* **2017**, *11*, 1380–1388

(3) Merino-Díez, N.; Li, J.; Garcia-Lekue, A.; Vasseur, G.; Vilas-Varela, M.; Carbonell-Sanromà, E.; Corso, M.; Guitián, E.; Ortega, J.E.; Peña, D.; Pascual, J.I.; de Oteyza, D. G. Unraveling the electronic structure of narrow atomically-precise chiral graphene nanoribbons. arXiv:1710.05813

(4) Kimouche, A.; Ervasti, M. M.; Drost, R.; Halonen, S.; Harju, A.; Joensuu, P. M.; Sainio, J.; Liljeroth, P. Ultra-Narrow Metallic Armchair Graphene Nanoribbons. *Nature Communications* **2015**, *6*, 10177

(5) Deniz, O.; Sánchez-Sánchez, C.; Dumslaff, T.; Feng, X.; Narita, A.; Müllen, K.; Kharche, N.; Meunier, V.; Fasel, R.; Ruffieux, P. Revealing the Electronic Structure of Silicon Intercalated Armchair Graphene Nanoribbons by Scanning Tunneling Spectroscopy. *Nano Letters* **2017**, *17*, 2197–2203